B-spline collocation simulation of non-linear transient magnetic nanobio-tribological squeeze-film flow

Beg, OA, Sohail, A, Kadir, A, Beg, T and Ravindran, Sabna

http://dx.doi.org/10.1142/S0219519418500070

Title	B-spline collocation simulation of non-linear transient magnetic nanobio-tribological squeeze-film flow
Authors	Beg, OA, Sohail, A, Kadir, A, Beg, T and Ravindran, Sabna
Type	Article
URL	This version is available at: http://usir.salford.ac.uk/id/eprint/44289/
Published Date	2018

B-SPLINE COLLOCATION SIMULATION OF NONLINEAR TRANSIENT MAGNETIC NANO-BIO-TRIBOLOGICAL SQUEEZE FILM FLOW

*O. Anwar Bég **

*Fluid Mechanics, Aeronautical and Mechanical Engineering, School of Computing, Science and Engineering, University of Salford, Newton Building, Manchester, M5 4WT, **UK.***

Ayesha Sohail

*Applied Mathematics Group, Department of Mathematics, COMSATS, Lahore, **Pakistan.***

Ali Kadir

*Structures and Materials, Aeronautical and Mechanical Engineering School of Computing, Science and Engineering, University of Salford, Newton Building, Manchester, M5 4WT, **UK.***

T.A. Bég

*Engineering Mechanics and Earthquake Engineering Research, Dickenson Rd., Manchester, M13, **UK.***

Sabna Ravindran

*MSc Aerospace Engineering Program, Aeronautical and Mechanical Engineering Department, University of Salford, Newton Building, Manchester, M5 4WT, **UK.***

Abstract

A mathematical model is presented for magnetized nanofluid bio-tribological squeeze film flow between two approaching disks. The nanofluid comprises a suspension of metal oxide nanoparticles with an electrically-conducting base fluid, making the nano-suspension responsive to applied magnetic field. The governing viscous momentum, heat and species (nano-particle) conservation equations are normalized with appropriate transformations which renders the original coupled, nonlinear partial differential equation system into a more amenable ordinary differential boundary value problem. The emerging model is shown to be controlled by a number of parameters, viz nanoparticle volume fraction, squeeze number, Hartmann magnetic body force number, disk surface transpiration parameter, Brownian motion parameter, thermophoretic parameter, Prandtl number and Lewis number. Computations are conducted with a B-spline collocation numerical method. Validation with previous homotopy solutions is included. The numerical spline algorithm is shown to achieve excellent convergence and stability in nonlinear bio-tribological boundary value problems. The interaction of heat and mass transfer with nanofluid velocity characteristics is explored. In particular smaller nanoparticle (high Brownian motion parameter) suspensions are studied. The study is relevant to enhanced lubrication performance in novel bio-sensors and intelligent knee joint (orthopaedic) systems.

Key Words: *Magnetic nanofluid; squeezing film; Brownian motion; B-spline collocation numerics; bio-tribology.*

*Corresponding Author- email: O.A.Beg@salford.ac.uk ; gortoab@gmail.com

1.INTRODUCTION

Nanofluids are suspensions of nanometre-sized particles in base fluids. Such fluids were introduced by Choi [1] and co-workers. The nanoparticles range from single-walled (SWCNT) and multi-walled carbon nanotubes, to metal oxides (gold, silver, titanium, copper etc) and fullerene, and these have been shown to consistently elevate the thermal conductivity characteristics of base fluids (e.g. silicon oil, ethylene glycol etc). Numerous and ever-diversifying applications of such fluids have been explored. In lubrication sciences, such fluids have demonstrated great promise in recent years. Many experimental and computational studies in this regard have been communicated. Hwang *et al.* [2] showed experimentally that thermal conductivity of nanofluid lubricants, which aids in heat dissipation, increases with increasing particle volume fraction and that extreme pressure sustainable by nanofluids increases up to 225%. Shen *et al*. [3] investigated water-based Aluminium oxide and diamond nanofluids in minimum quality lubrication (MQL) grinding processes, showing that nanofluids dramatically decrease grinding forces, enhance surface roughness and mitigate workpiece burning. Khandekar *et al.* [4] studied performance of nano-cutting fluids (suspensions of ordinary cutting fluid and nanoparticles) using a macroscopic contact angle technique, demonstrating that introduction of nanoparticles successfully improves wettability, lubricating properties, and convective heat transfer coefficient (cooling properties) of nano-cutting fluids. They also found that nanofluids decrease workpiece surface roughness, tool wear and chip thickness compared with conventional dry machining or conventional cutting fluids. Mao *et al.* [5] used a pin-on-flat tribotester to investigate nanoparticles effects (Aluminium oxide) in nanofluid lubrication, showing that significant friction reduction is achieved and better anti-wear properties. Pendleton *et al.* [6] studied nanostructured fullerene and other particle additives in nanofluid tribological performance of titanium and its alloys for medical orthopedic applications. Sahoo *et al.* [7] employed Molybdenum sulphate nanoparticles to improve sliding lubrication in journal bearings. Nicoletti [8] utilized copper and silicon oxide nanoparticles, among others, to study thermal dissipation performance in nano-lubricants showing that greater volumetric heat capacity of the lubricant decreases temperature development in the bearing gap, leading to elevated viscosity distribution for the same operating conditions. Numerous other studies have

been communicated including Harta *et al.* [9] who used zinc oxide nanoparticle-oil nanofluids for metal-on-metal contacts, Wasan and Nikolov [10] who investigated spreading and adhesion charactersitics of nanofluids on solid surfaces with surfactant micelles, Binu *et al*. [11] who employed Titanium oxide nano-lubricants, Xu *et al.* [12], Kumar and Bushan [13] who considered commercial coatings of diamond-like-carbon and other materials for nitriding treatment on H-13 steel and Niyaghi *et al.* [14] who used zinc oxide metalworking nanofluids. Ghaednia *et al.* [15] conducted experiments on Copper oxide nanoparticles suspended in mineral base oil, using sodium oleate as a surfactant, observing that boundary lubricant temperature is decreased and viscosity of the nano-lubricants is enhanced with addition of more nanoparticles. Kang *et al.* [16] reported on performance-enhancing properties of Iron Nickel nanoscale fluids.

Within tribology, *squeeze film flows* are frequently encountered. They arise in machine elements, automotive components, prosthetics, aerospace and bridge dampers, matching gears, wet-clutch plates etc. In general, research of squeeze film characteristics concentrates attention on the use of Newtonian lubricants and modifications of Reynolds celebrated equation. However a separate group of problems also arises in which nonlinear partial differential equation systems for the regime may be formulated and solved, often for non-Newtonian and other complex lubricants. Such "thin layer" boundary value problems are of great interest to computational mechanics researchers. An extensive range of numerical algorithms have been applied in recent years to study multi-physical squeeze-film problems. Magnetohydrodynamic squeeze films have in particular garnered much attention owing to developments in smart systems. Hayat *et al*. [17] used a homotopy analysis technique to study magneto-micropolar squeeze films. Bég *et al*. [18] used an Adomian decomposition code to investigate magnetic squeeze film lubrication at generalized Batchelor numbers. Daliri *et al.* [19] used MATLAB software to simulate squeeze film magnetic non-Newtonian flows in wide parallel rectangular conjunctions, showing that magneto-hydrodynamic couple stress fluids are more appropriate for high relatively steady load applications. Zueco and Bég [20] employed thermo-electric code, PSPICE to simulate magnetic Newtonian squeeze films in a dual-disk spinning lubrication system. Hayat *et al.* [21] used homotopy methods to study magnetic viscoelastic squeeze films. Bég *et al.* [22] studied gyration viscosity and squeeze number

effects on unsteady magnetized micropolar squeeze films in helicopter damper systems, with a meshless numerical method.

The above studies [17-22] however did not consider *nanofluid* lubricants. In the present work we address magnetized nanofluid squeeze film flow in dual disk systems. A robust B-spline collocation numerical method is employed to solve the transformed nonlinear boundary value problem. Validation with earlier homotopy solutions is included. The current study is motivated by potential applications of magnetic nano-lubricants in heat dissipation and better flow control in dampers [23, 24]. We examine in detail the radial velocity evolution and modification by surface blowing/suction, nanofluid and magnetic field characteristics in magnetic nanofluid squeeze film flow between two parallel circular disks, one solid and the other porous. Solutions are further benchmarked with earlier homotopy solutions [25] where possible, although these are limited in the range of parameters examined. The present study also provides a useful benchmark for more complex computational fluid dynamics simulations with commercial software e.g. ADINA-F, FLUENT etc [26] and furthermore, it is hoped that it will stimulate some interest from experimental researchers engaged in nano-magnetic lubrication engineering in the medical arena.

2. MAGNETIZED NANO-BIO-TRIBOLOGICAL SQUEEZE FILM MODEL

The physical regime under investigation is illustrated in **Fig. 1**. Transient incompressible magnetized bio-nanofluid flow occurs between two parallel circular plates, in an (r, θ, z) coordinate system. The disks are parallel to the r-θ plane, with the z-axis normal to this plane. A magnetic field, $B(t) = B_o(1\text{-}at)^{-1/2}$ is applied along the z-axis. The magnetic Reynolds number is small for the magneto-nano-lubricant regime, so that magnetic induction effects can be ignored. The disks are separated by a distance $h(t) = H(1 - at)^{1/2}$. The upper disk at $z = h(t)$ descends towards/ascends away from the stationary lower disk with the velocity $dh=dt$. The surface temperature and nanoparticle concentrations on both disks are constant and defined by T_w, C_w *(lower)* and T_h, C_h *(upper)*, respectively. A constant transpiration velocity, w_o, is present at the lower disk; the upper disk is impervious. The conservations equations for mass, radial and axial momentum, heat and

nanoparticle concentration (species diffusion) may be presented, following Hashmi *et al.* [25]:

Mass Conservation

$$\frac{\partial u}{\partial r} + \frac{u}{r} + \frac{\partial w}{\partial z} = 0 \tag{1}$$

r-direction Momentum Conservation

$$\frac{\partial u}{\partial t} + u\frac{\partial u}{\partial r} + w\frac{\partial u}{\partial z} = -\frac{1}{\rho_{nf}}\frac{\partial p}{\partial r} + \nu\left(\frac{\partial^2 u}{\partial r^2} + \frac{\partial^2 u}{\partial z^2} + \frac{1}{r}\frac{\partial u}{\partial r} - \frac{u}{r^2}\right) - \frac{\sigma}{\rho_{nf}}B^2(t)u \tag{2}$$

z-direction Momentum Conservation

$$\frac{\partial w}{\partial t} + u\frac{\partial w}{\partial r} + w\frac{\partial w}{\partial z} = -\frac{1}{\rho_{nf}}\frac{\partial p}{\partial z} + \nu\left(\frac{\partial^2 w}{\partial r^2} + \frac{\partial^2 w}{\partial z^2} + \frac{1}{r}\frac{\partial w}{\partial r}\right) \tag{3}$$
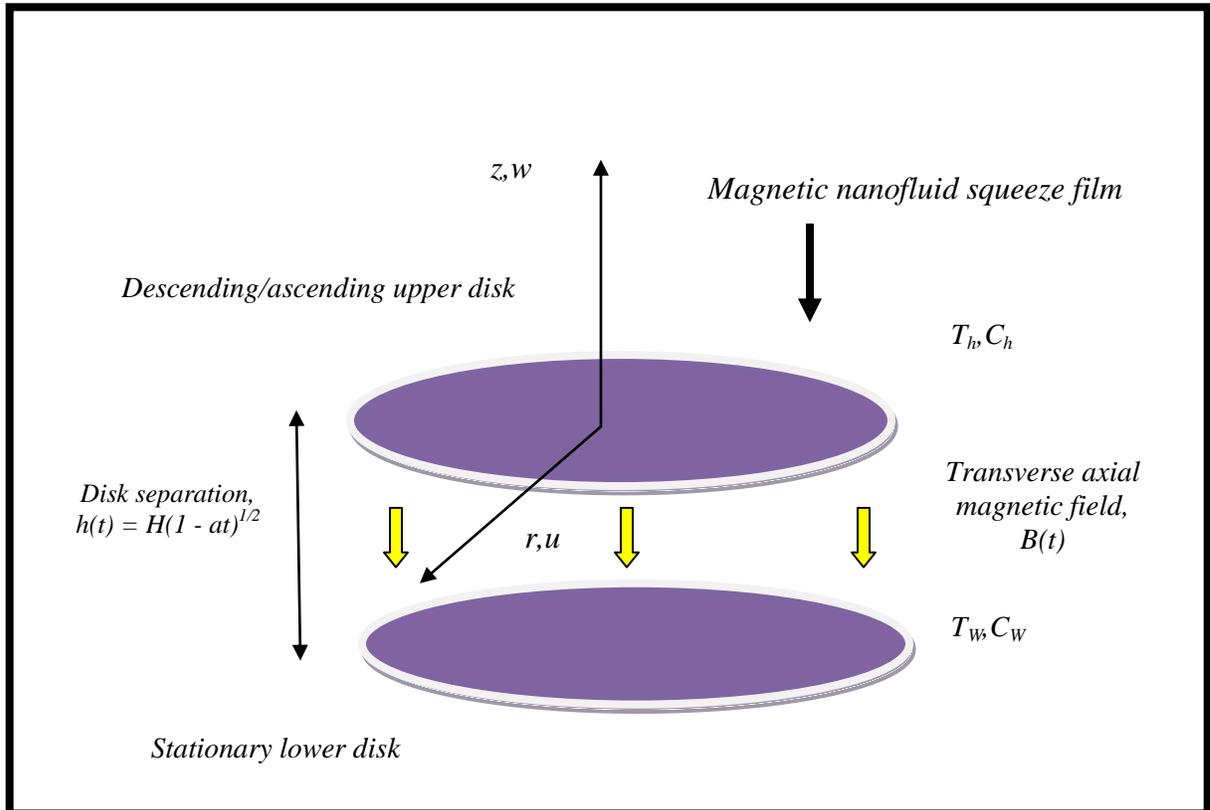

Figure 1: Physical Model and Coordinate System

Energy (Heat) Conservation

$$\frac{\partial T}{\partial t} + u\frac{\partial T}{\partial r} + w\frac{\partial T}{\partial z} = \alpha(\frac{\partial^2 T}{\partial r^2} + \frac{1}{r}\frac{\partial T}{\partial r} + \frac{\partial^2 T}{\partial z^2})$$
$$+ \tau\{D_B(\frac{\partial C}{\partial r}\frac{\partial T}{\partial r} + \frac{\partial C}{\partial z}\frac{\partial T}{\partial z}) + \frac{D_T}{T_m}([\frac{\partial T}{\partial r}]^2 + [\frac{\partial T}{\partial z}]^2)\}$$

(4)

Nano-particle Species Conservation

$$\frac{\partial C}{\partial t} + u\frac{\partial C}{\partial r} + w\frac{\partial C}{\partial z} = D_B(\frac{\partial^2 C}{\partial r^2} + \frac{1}{r}\frac{\partial C}{\partial r} + \frac{\partial^2 C}{\partial z^2}) + \frac{D_T}{T_m}(\frac{\partial^2 T}{\partial r^2} + \frac{1}{r}\frac{\partial T}{\partial r} + \frac{\partial^2 T}{\partial z^2})$$

(5)

We note that in Eq. (5), which is a statement of Fick's law of mass (species) diffusion for nanoparticles, the first term on the left hand side is the *transient concentration gradient*, and the second and third terms are the convective mass transfer terms. The first bracketed term on the right hand side denotes the *species diffusion* and the last bracketed term is the relative *contribution of thermophoresis to Brownian motion*. The corresponding boundary conditions for the flow regime are prescribed as follows, which include the conventional no-slip boundary conditions at the disk surfaces:

At $z = h(t)$: $u=0$; w $=dh/dt$; $T=T_h$; $C=C_h$ (6a)

At $z = 0$: $u=0$; $w=-w_o/\surd(1-at)$; $T=T_w$; $C=C_w$ (6b)

where *u, w* are radial and axial velocity components respectively, *t* is time, ρ_{nf} is the nanofluid density, μ is the dynamic viscosity of the nanofluid, *p* is pressure, *T* denotes nanofluid temperature, *C* is nanoparticle concentration (volume fraction), α is thermal diffusivity of nanofluid, D_B is the Brownian motion coefficient (species diffusivity of nanoparticles), D_T is thermophoresis diffusion coefficient (relating to particle deposition induced by a temperature gradient), T_m denotes mean fluid temperature, *k* is nanofluid thermal conductivity, T_h is upper disk surface temperature, T_w is lower disk surface temperature, C_h is upper disk surface nano-particle concentration, C_h is lower disk surface nano-particle concentration, w_o is lower disk lateral mass flux velocity (suction/injection), τ designates the ratio of effective heat capacity of nanoparticles to heat capacity of the

base fluid (a function of the type of nanomaterial e.g. copper oxide, titanium oxide, silicon oxide etc). Computational solutions to the nonlinear boundary value problem defined by eqns. (1)-(6) while tractable, are challenging. It is judicious to introduce normalization variables as similarity parameters which not only simplify the conservation equations, but introduce a set of important dimensionless parameters which provide interesting insights to the squeeze film mechanisms. Defining the following *dimensionless* variables:

$$u = \frac{ar}{2(1-at)}\frac{dF}{d\eta}; \; w = -\frac{aH}{\sqrt{1-at}}F(\eta); \eta = \frac{z}{H\sqrt{1-at}};$$

$$B(t) = \frac{Bo}{\sqrt{1-at}}; G(\eta) = \frac{T-T_h}{T_w-T_h}; N(\eta) = \frac{C-C_h}{C_w-C_h}$$

(7)

The conservation equations then retract to the following ordinary differential equations:

Momentum conservation

$$\frac{d^4F}{d\eta^4} - S(\eta\frac{d^3F}{d\eta^3} + 3\frac{d^2F}{d\eta^2} - 2F\frac{d^3F}{d\eta^3}) - Ha^2\frac{d^2F}{d\eta^2} = 0$$

(8)

Heat conservation

$$\frac{d^2G}{d\eta^2} + \Pr S(2F\frac{dG}{d\eta} - \eta\frac{dG}{d\eta}) + \Pr Nb\frac{dG}{d\eta}\frac{dN}{d\eta} + \Pr Nt(\frac{dG}{d\eta})^2 = 0$$

(9)

Nanoparticle species conservation

$$\frac{d^2N}{d\eta^2} + LeS(2F\frac{dN}{d\eta} - \eta\frac{dN}{d\eta}) + \frac{Nt}{Nb}\frac{d^2G}{d\eta^2} = 0$$

(10)

The associated boundary conditions for the squeezing flow contract to the following form:

At $\eta = 1$ *(Upper disk)*: $F(1) = 0.5$; $dF(1)/d\eta = 0$; $G(1) = N(1) = 0$ (11a)

At $\eta = 0$ *(Lower disk)*: $F(0) = A$; $dF(0)/d\eta = 0$; $G(0) = N(0) = 1$ (11b)

A number of key parameters emerge in the new similarity equations and boundary conditions, and these take the following definitions:

$$A = \frac{w_o}{aH}; S = \frac{aH^2}{2v}; Ha = \sqrt{\frac{\sigma B_0^2 H^2}{v}}; \Pr = \frac{v}{\alpha}; Le = \frac{v}{D_B};$$

$$Nb = \frac{(\rho c)_p D_B (C_w - C_h)}{(\rho c)_f v}; Nt = \frac{(\rho c)_p D_T (T_w - T_h)}{(\rho c)_f T_m v} \qquad (12)$$

Here A is the lower disk transpiration parameter ($A>0$ implies suction; $A<0$ corresponds to blowing), S is the squeezing number, Ha is the Hartmann magnetic body force number (ratio of Lorentz radial magnetic drag force to the viscous hydrodynamic force), Pr is Prandtl number, Le is Lewis number, Nb is Brownian motion parameter, Nt is thermophoresis parameter. We may also define key surface parameters, namely surface radial shear stress (disk skin friction), C_{fr}, Nusselt number, Nu_r, (disk surface heat transfer rate) and Sherwood number, Sh_r, (disk surface mass transfer rate) as follows:

$$C_{fr} = \frac{<\tau_{rz}>_{z=h(t)}}{\rho\left(\frac{-aH}{2(1-at)^{1/2}}\right)^2}; Nu_r = \frac{Hq_w}{k(T_w - T_h)}; Sh_r = \frac{Hj_w}{D_B(C_w - C_h)} \qquad (13)$$

Where:

$$\tau_{rz} = \mu\left(\frac{\partial u}{\partial z} + \frac{\partial w}{\partial r}\right)_{z=h(t)}; q_w = -k\left(\frac{\partial T}{\partial z}\right)_{z=h(t)}; j_w = -D_B\left(\frac{\partial C}{\partial z}\right)_{z=h(t)} \qquad (14)$$

In terms of the dimensionless variables (7), the non-dimensional upper disk shear stress, reduced heat transfer rate and reduced nanoparticle (mass) transfer rate take the form:

$$\frac{d^2 F(1)}{d\eta^2} = \frac{H^2}{r^2} \text{Re}_r C_{fr};$$

$$-\frac{dG(1)}{d\eta} = Nu_r = (1-at)^{1/2} Nu; \qquad (15)$$

$$-\frac{dN(1)}{d\eta} = Sh_r = (1-at)^{1/2} Sh$$

Where a *radial Reynolds number* is used and defined as, $\text{Re}_r = \frac{raH(1-at)^{1/2}}{2v}$. We note that a *non-dimensional load carrying capacity* and *time of approach* can also be derived to simulate squeezing effects and tribological performance.

3. B-SPLINE COLLOCATION NUMERICAL SOLUTIONS

This method reduces the computational cost on a large domain with small step size and a range of parameters. For the application of the spline collocation method, the system of differential equations (8-10) can thus be rendered into a simpler system of differential equations:

$$w_x^{ns}(\eta) = f(\eta; z(w)) \tag{16}$$

Here:

$$0 \leq \eta \leq 1; \; n_s = 4,2,2 \; for \; s = 1,2,3. \tag{17}$$

The numerical solver will produce the following vector solution:

$$\boldsymbol{w} = [w_1, w_2, w_3]^T \tag{18}$$

$$z(\boldsymbol{w}) = [w_1, w_1', w_1'', w_1''', w_2, w_2', w_3, w_3'] \tag{19}$$

After simplifying the system of differential equation(s) (16) as a function (f_s; s=1, 2, 3) of the independent variable, η, and the function $z(w)$, under the boundary conditions (11a-11b), we obtain the desired numerical solution. The method of spline collocation at Gaussian points using a B-spline basis has been implemented to calculate the B-splines and their derivates. The matrix has been simplified using the Gaussian elimination with partial pivoting [29]. B-Splines employ the mathematical principle of splines which are continuous piecewise curves used to approximate a solution to a mathematical problem. A spline curve is dependent upon a relationship between the basis function and the vertices of a defining polygon. The B-spline curve has its own type of basis function, known as the B-spline basis, to establish the relationship with the defining polygon. Many other types of splines are employed in numerical analysis including the Bezier spline (which deploys a Bernstein basis function to establish the relationship). However, the B-spline basis function is advantageous in that the order of the base function can be reduced, resulting in curves with a lower degree, without the penalty of a reduction in approximation accuracy. This allows increased computational speed and less memory

requirements during compilation. Furthermore B-splines allow relatively easy local refinement to the function. The nonlinear parts of the system are dealt by the use of a modified-Newton method. The mesh refinement has been controlled by the redistribution of mesh points for better accuracy and hence to reduce the error. To validate the B-spline numerical solutions, we benchmark against the earlier HAM solutions in [25]- see **Tables 1 and 2**.

Table 1: Benchmark solutions for upper disk surface friction with Nt=Nb=0.1, Le=1, Pr = 1, A= 2, for various values of Hartmann number and squeeze number.

Ha	S	$\dfrac{d^2 F(1)}{d\eta^2}$ (HAM [25])	$\dfrac{d^2 F(1)}{d\eta^2}$ (B-Spline collocation)
0	1	7.533165	7.532158
2	"	8.263872	8.241627
3	"	9.097326	9.095184
5	"	11.34929	11.337581
1	1	7.721946	7.718385
	2	6.940773	6.939045

Table 2: Benchmark solutions for reduced Nusselt number and reduced Sherwood number for various Nt and Nb with A=2, Ha=S=Le=Pr =1.0.

Nb	Nt	$-\dfrac{dG(1)}{d\eta}$ (HAM [25])	$-\dfrac{dG(1)}{d\eta}$ (B-Spline collocation)	$-\dfrac{dN(1)}{d\eta}$ (HAM [25])	$-\dfrac{dN(1)}{d\eta}$ (B-Spline collocation)
0.1	0.1	0.5263	0.5192	0.8660	0.8657
0.5	"	0.6343	0.63414	0.5301	0.5298
1	"	0.7864	0.78644	0.4860	0.4856
1.5	"	0.9557	0.9556	0.4698	0.4696

"	0.5	1.1768	1.1767	0.4018	0.4016
"	1.0	1.4858	1.4849	0.1261	0.1256

Inspection of the tables reveals that very close correlation is achieved between the present B-Spline collocation approach and established homotopy solutions in the literature. Confidence in the B-spline collocation solutions is therefore justifiably high. **Table 1** shows that as Hartmann number (Ha) increases (with squeeze parameter, S, invariant at unity), there is a significant elevation in the upper disk friction, $\dfrac{d^2F(1)}{d\eta^2}$. As Hartmann number is elevated, there is a corresponding increase in magnetic field, based on the definition of Ha in eqn. (12). The magnetic body force term, $-Ha^2\dfrac{d^2F}{d\eta^2}$, in the momentum conservation eqn. (8) is inhibiting to the radial squeeze film flow (which is perpendicular to the line of application of the magnetic field in the axial direction). Via this Lorentzian drag force, the radial squeeze film flow is decelerated and this manifests in a enhancement of shear stress at the disk i.e. upper disk surface friction. With increasing squeeze film number, S, the converse response is observed and disk friction is markedly decreased. This implies that as the disk separation is increased (or as viscosity is decreased) the flow is accelerated, and this results in a decrease in shear stress i.e. disk friction. Evidently both Hartmann number and squeeze number are instrumental parameters in regulating the flow and particularly important since they can be manipulated relatively easily in real designs to achieve a desired performance. **Table 2** shows that with increasing Brownian motion parameter (Nb) there is a considerable increase in heat transfer rate i.e. reduced Nusselt number, $-\dfrac{dG(1)}{d\eta}$, at the upper disk. Greater Brownian motion therefore aids in the transport of thermal energy from the bio-lubricant to the disk which achieves the desired effect of cooling the squeeze film. Conversely the mass transfer rate i.e. rate of nano-particle diffusion to the upper disk, $-\dfrac{dN(1)}{d\eta}$ i.e. reduced Sherwood number is substantially lowered. This is a result of enhanced diffusion of nano-particles into the body of the squeeze film i.e. greater

concentration within the bio-lubricant. This is consistent therefore with the enhanced migration of nano-particles *away* from the upper disk. With greater thermophoretic parameter (*Nt*), the reduced Nusselt number at the upper disk is depressed. However there is a much more profound elevation in local Sherwood number. Thermophoresis is related to the encouraged trans-location of nano-particles under the force of a temperature gradient. The enhanced heat transfer rate to the upper disk displaces nano-particles away from this zone. These nano-particles in the lubricant create an accelerated flow down the temperature gradient and this results in a noticeable decrease in nano-particle mass transfer rate to the upper disk i.e. decreasing reduced Sherwood number. The migration of nano-particles back into the main body of the squeeze film is also advantageous since more homogenous distributions can be achieved and better global cooling of the nano-lubricant is sustainable, a key desire of bio-tribologists.

4. B-SPLINE NUMERICAL SIMULATION RESULTS AND DISCUSSION

Extensive computations have been conducted for a comprehensive range of the key bio-tribological and nanoscale parameters. The present investigation considerably extends the analysis performed by Hashmi *et al*. [25] and in particular provides deeper interpretation of computations, which is of great interest to bio-tribologists.
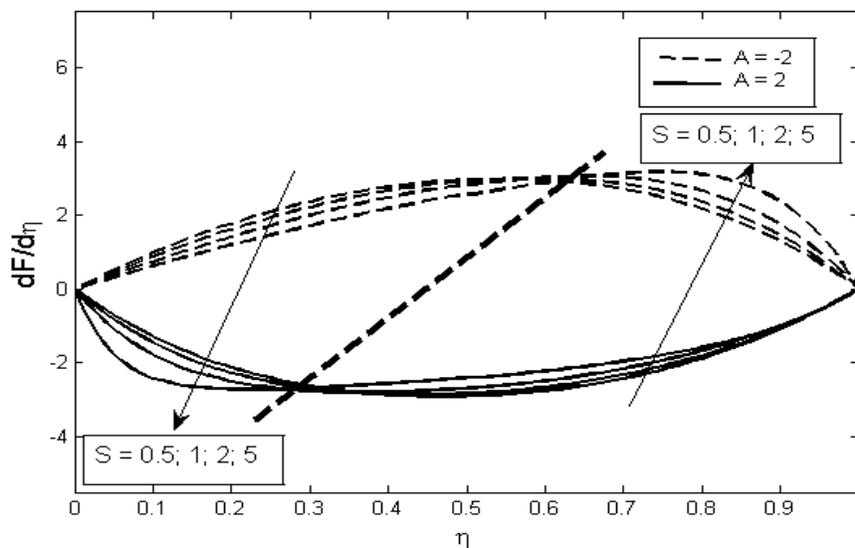

Fig. 2: Radial velocity distribution (dF/dη) versus transverse coordinate (η) for various wall transpiration parameters (*A*) and various squeeze film parameters *(S) with Le*=1, *Pr = 1, Nb = Nt = 0.2, Ha=2.*

Fig. 2 depicts the evolution of radial velocity with different transpiration and squeeze film parameter values. With wall blowing present at the disk (*A*<0) there is a significant enhancement in velocity compared with wall suction (*A*>0).
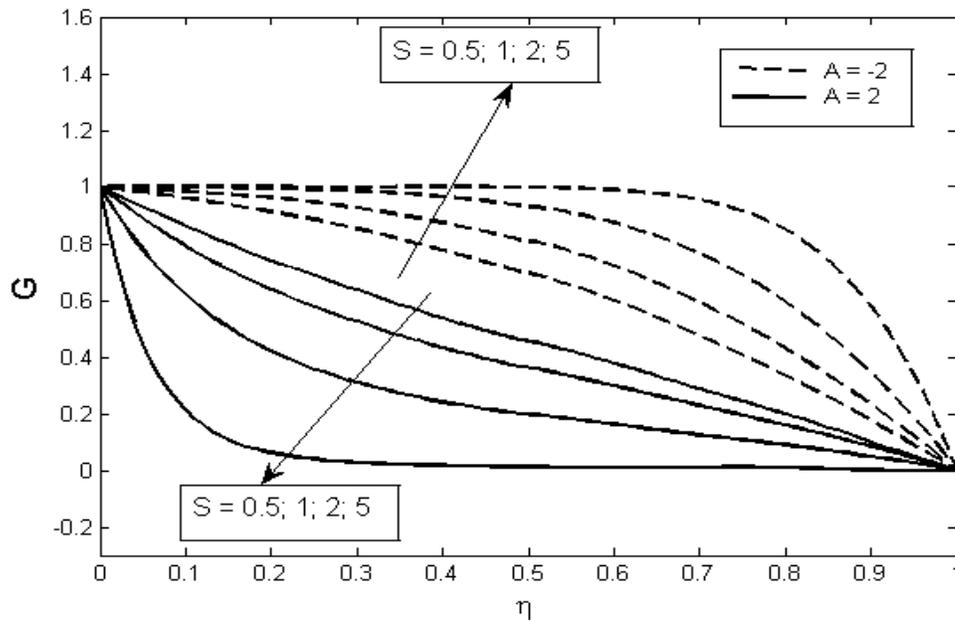

Fig. 3: Temperature distribution (*G*) versus transverse coordinate (*η*) for various wall transpiration parameters (*A*) and squeeze film parameters *(S) with Le*=1, *Pr = 1, Nb = Nt = 0.2, Ha=2.*
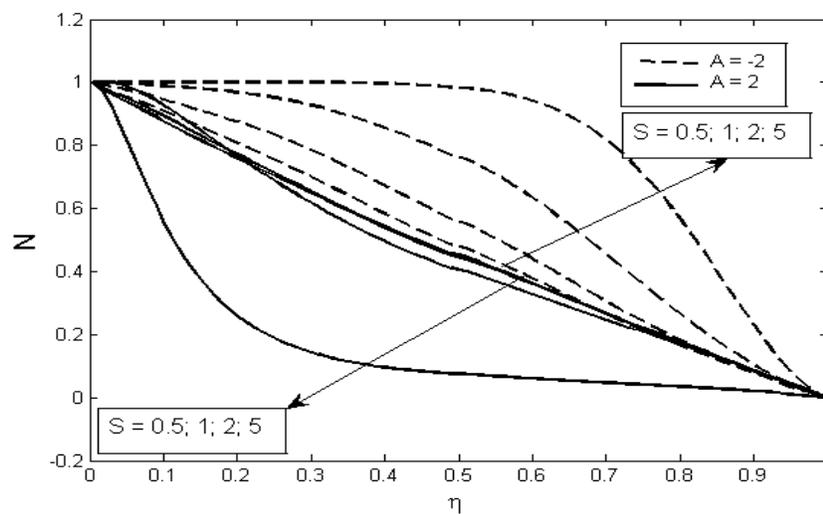

Fig. 4: Nano-particle concentration distribution (*N*) versus transverse coordinate (*η*) for various wall transpiration parameters (*A*) and squeeze film parameters *(S) with Le*=1, *Pr = 1, Nb = Nt = 0.2, Ha=2.*
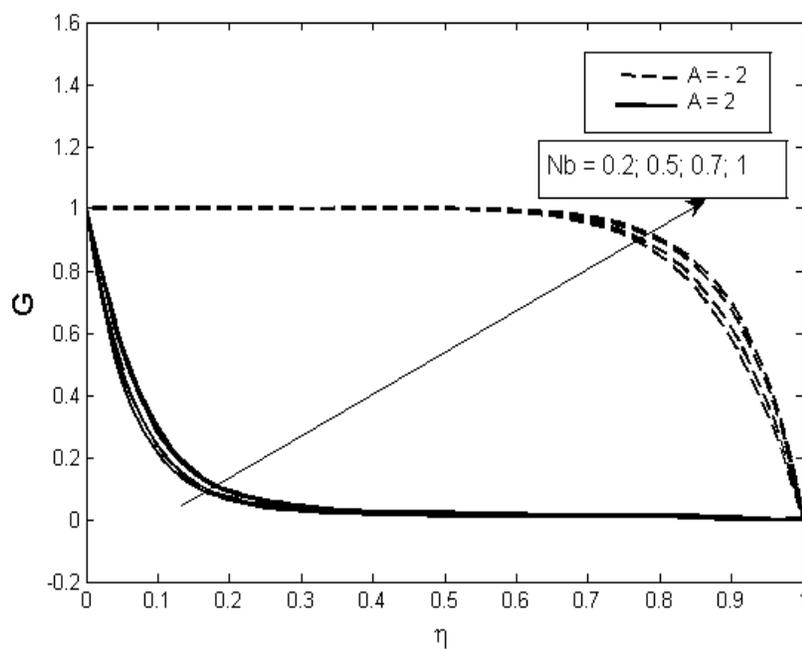
Fig. 5: Temperature (*G*) versus η for *Le*=1, *Pr =1, Nt = 0.2, Ha=2, S= 1 with various Brownian motion numbers (Nb) and transpiration parameters (A).*
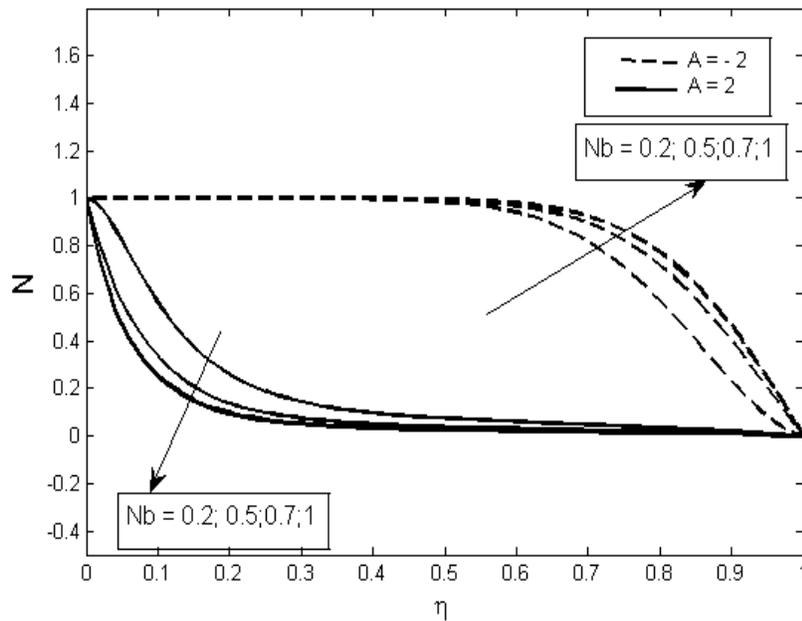

Fig. 6: Nano-particle concentration distribution (*N*) versus η for *Le*=1, *Pr =1, Nt = 0.2, Ha=2, S= 1 with various Brownian motion numbers (Nb) and transpiration parameters (A).*
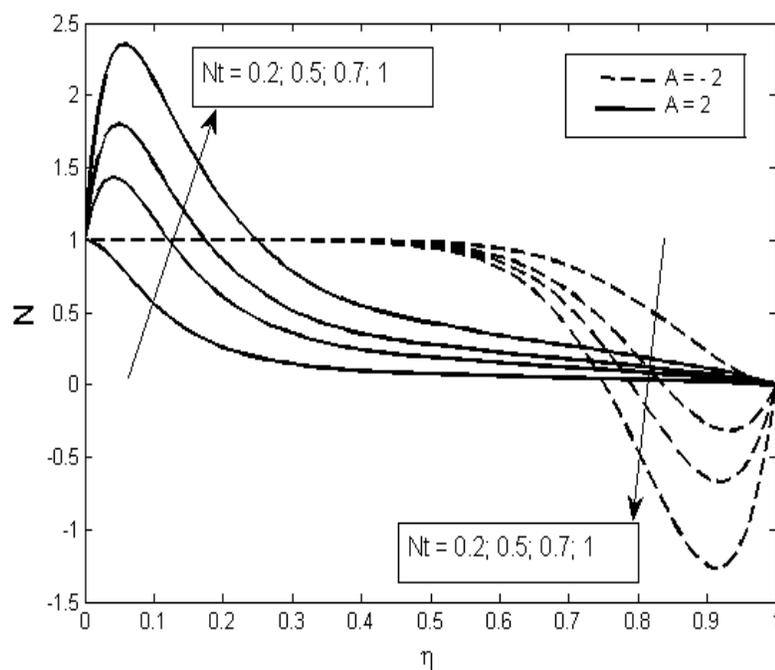
Fig. 7: Nano-particle concentration distribution (*N*) versus η for *Le*=1, *Pr* =1, *Nb = 0.2, Ha=2, S= 1 with various thermophoretic numbers (Nt) and transpiration parameters (A).*
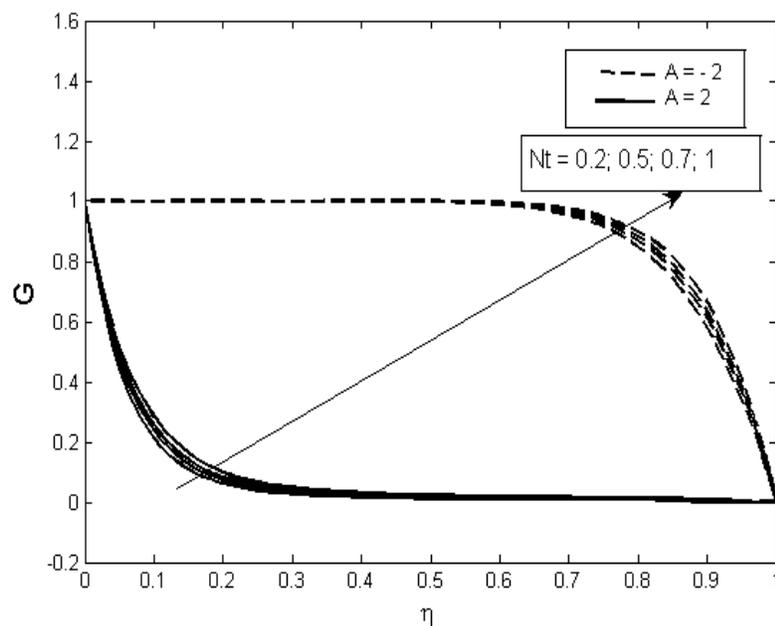

Fig. 8: Temperature (*G*) versus η for *Le*=1, *Pr* =1, *Nb = 0.2, Ha=2, S= 1 with various thermophoretic numbers (Nt) and transpiration parameters (A).*
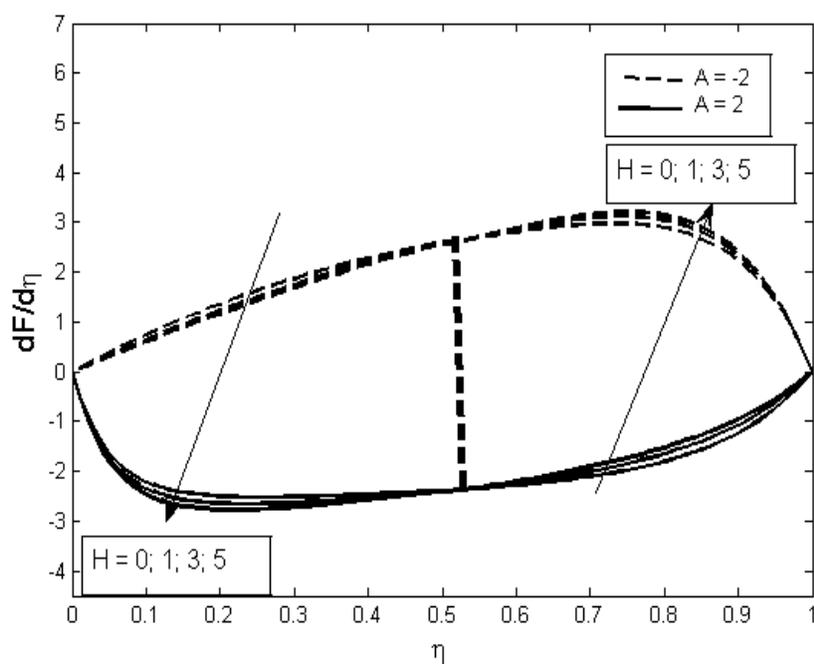
Fig 9: Radial velocity distribution versus η for *Le=1, Pr =1, Nb = 0.2, Nt =0.3, A= 1, S= 1 with various Hartmann numbers (Ha) and transpiration parameters (A).*
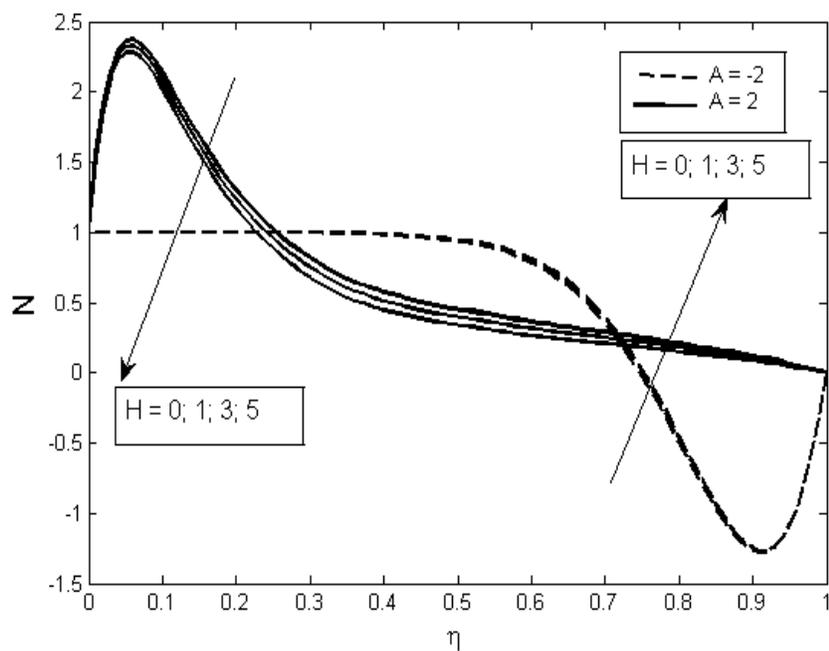

Fig 10: Nano-particle concentration (*N*) distribution versus η for *Le=1, Pr =1, Nb = 0.2, Nt =0.3, A= 1, S= 1 with various Hartmann numbers (Ha) and transpiration parameters (A).*

The latter i.e. suction, causes *adherence of the squeeze film* to the disk surfaces and destroys momentum in the regime. The former i.e. *blowing (injection)* adds more bio-lubricant via perforations in the disk surfaces to the squeeze film and this serves to accelerate the flow. Lateral mass flux via geometrical modification of the disk surface using machined pores is therefore a potent mechanism for controlling the flow in the squeeze film.

Fig. 3 presents temperature profiles in the disk gap for various transpiration (*A*) and squeeze film parameter (*S*) values. There is a general decay in temperatures from the lower disk to the upper disk which becomes increasingly monotonic in nature (i.e. progressively less linear) with increasing squeeze film parameter. Greater squeezing effect therefore stifles temperatures and inhibits thermal diffusion in the nano-lubricant. This has important implications in sustaining cooling in the regime, which prolongs lubricant life. A similar response was computed by Hashim *et al.* [25] and furthermore has also been reported by Zhao *et al.* [30] and Mivake *et al.* [31]. The behaviour is similar to conventional lubricants, however the temperature reduction is more dramatic. With increasing suction effect at the disk, temperature is also significantly lower in magnitude than with transpiration. Furthermore with transpiration present, the supplementary injection of nano-lubricant into the gap serves to elevate temperatures with greater squeeze parameter. The squeezing effect is therefore reversed and for high *S* values, the profiles becoming increasingly parabolic i.e. they deviate from the gentler parabolic decays associated with lower *S* values.

Fig. 4 illustrates the response in nano-particle concentration (*N*) with the combined effects of transpiration (*A*) and squeeze film parameter (*S*). As with temperature field, a significant suppression in *N* values is observed, with disk wall suction present (*A*= 2). For low squeeze parameter (*S*=0.5), the decay in nano-particle concentration is approximately linear. It evolves into a strongly parabolic distribution for high *S* values. Nano-particle concentrations achieve a maximum at the lower disk (η=1) and consistently a minimum at the upper disk (η=1). The Brownian motion (*Nb*=0.2) and thermophoresis parameter (*Nt* = 0.2) values prescribed are high and correspond to smaller nano-particles. With wall transpiration present (*A* =-2), the influence of increasing squeeze film parameter is reversed and nano-particle concentration magnitudes are significantly elevated. The

addition of lateral mass of nano-lubricant via the disk surfaces therefore assists in nano-particle diffusion across the gap and disperses nano-particles more evenly between the two disks.

Figs 5 and 6 illustrate the collective influence of transpiration parameter (A) and Brownian motion number (Nb) on temperature and nano-particle species distribution in the disk gap. A non-trivial elevation in the temperature (fig. 5) is induced either with suction present or injection present, with an increase in Nb values. However significantly greater magnitudes are attained with disk injection (blowing) across the entire inter-disk gap zone. There is an approximate reflective symmetry in the profiles for suction or injection present. Maximum temperature enhancement is achieved closer to the lower disk, with wall suction present and a short proximity from the lower disk, there is an asymptotic convergence in all the temperature profiles. Conversely with transpiration present, the maximum boost in temperature arises in the vicinity of the upper disk, with all profiles converging to a single value at the lower disk. Experimental works have also demonstrated similar findings, notably the study by Liu and Wang [32] and Kulkarni *et al.* [33], both considering metallic nano-particles, which are consistent with the model developed in the present article. The presence of wall injection also serves to enhance notably the nano-particle concentration (N), as shown in fig. 6, whereas disk wall suction generates significant reduction in N magnitudes. The reflective symmetry observed in temperature profiles is again present in the N-profiles. Increasing Brownian motion number, Nb however only enhances nano-particle concentration when wall injection is present, whereas it depresses concentration when wall suction is present. The influence of Brownian motion on nano-particle species diffusion is therefore dependent on the transpiration scenario at the disk, whereas for temperature it is independent. It has been observed experimentally [34] that for very small nanoparticles (i.e. higher Nb values), the random "walk" component of the particle displacement is of a similar order of magnitude to the displacement associated with the particle diffusion due to the interparticle repulsive forces. Brownian motion is the random thermally driven movement of particles suspended in the nano-lubricant. This random motion serves to convey energy directly by nanoparticles in addition to the micro-convection effect, which is attributable to the fluid mixing around nanoparticles. The exacerbated motion at higher Nb values is assisted with

the momentum boost (transpiration) whereas it is inhibited by momentum destruction (wall suction). Of course, there are many other factors which influence Brownian motion including the geometry of nano-particles, ballistic collisions and further experimental studies are required to exactly establish how these characteristics are modified in squeeze films [35]. Indeed molecular dynamics simulation may also provide an insight into these complex mechanisms in lubrication applications [36].

Figs. 7 and 8 illustrate the influence of thermophoresis parameter (*Nt*) and transpiration parameter (*A*) on respectively the nano-particle concentration and temperature profiles. A significant elevation is observed in the nano-particle concentrations (fig. 7) near the lower disk with increase in thermophoresis effect, with wall suction present (*A*=2). This growth in profiles is sustained to the upper disk although magnitudes decay quickly beyond the gap centre line. Conversely with increasing *Nt* values, and wall injection present at the disk, there is significant reduction in nano-particle concentrations, in particular close to the upper disk. Peak nano-particle concentration is computed therefore for strong suction and high *Nt* value, near the lower disk, whereas the minimum nano-particle concentration arises for strong injection (blowing), near the upper disk, again with high *Nt* (=0.7). As elaborated earlier thermophoresis is experienced by the nano-particles owing to the thermophoretic force which acts in a direction opposite to the imposed temperature gradient, in the nano-lubrication squeeze film. Even though the fluid zone is confined, the thermophoresis effect is still prominent. It also exerts a different influence depending on the nature of the lateral mass flux at the disks i.e. whether suction or injection is present. Generally to achieve greater magnitudes and more homogenous distributions of nano-particles across the squeeze film gap, strong thermophoresis and suction are effective, however only in the vicinity of the lower disk (note in the boundary conditions 11a,b, transpiration is only imposed *at the lower disk* which is stationary; the upper disk which descends, is impervious). Temperature (fig. 8) is affected to a much lesser extent than nano-particle concentration. Thermophoresis parameter, *Nt* arises in both energy (heat) and nano-particle species conservation equations i.e. eqns. (9) and (10), in the terms $\Pr Nt(\frac{dG}{d\eta})^2$ and $\frac{Nt}{Nb}\frac{d^2G}{d\eta^2}$. Both terms evidently exert a significant effect. However in the latter there is also a Brownian motion

parameter present. This leads to a more erratic response in the nano-particle concentration field than in the temperature field. Generally temperature is increased with greater thermophoretic effect, irrespective of whether suction or injection is prescribed at the lower disk. However the temperature magnitudes are significantly higher with injection (blowing) than they are for suction. *Cooling of the squeeze film* is therefore more effective when *wall suction* is applied at the lower disk and when *weak thermophoresis* is present. The temperature field is influenced in a more orderly fashion than the nano-particle concentration (fig. 7). In these computations, Prandtl number has been fixed at unity indicating that the energy and species diffusion rates are of the same order of magnitude. This is representative of certain bio-nano-lubricants as described in [35].

Figs. 9, 10 present the evolution of velocity and nano-particle concentration distributions with Hartmann number (*Ha*) and transpiration parameter (*A*). Significant radial flow deceleration is achieved with an increase in Hartmann number when suction is present at the lower disk, as observed in fig. 9. However the converse behavior is observed with injection at the lower disk, and furthermore markedly greater velocities are computed with injection than with suction. The nature of the applied magnetic field, which is axially orientated, is to generate a transverse Lorentzian magnetohydrodynamic drag force. This acts in the radial direction and when Hartmann number increases, this drag force is accentuated. This leads to a retardation in radial velocity. The effect is however only achieved with suction present. However with injection present (wall blowing at the lower disk i.e. *A* =-2), the introduction of mass flux into the squeeze film regime counter-acts the inhibiting nature of the magnetic field and in fact accelerates the radial flow. For bio-tribologists, therefore suction is best combined with strong magnetic field (Hartmann number is a function of magnetic field), to achieve greater control of the squeeze film dynamics. Similarly we observe in fig. 10, that the nano-particle concentration is also decreased with greater Hartmann number, when suction is present at the lower disk. Although the reduction is significantly less prominent than the radial velocity field (fig. 9) it is still substantial. With wall injection present, however a very weak increase is computed in nano-particle concentration and the modifications to profiles are most pronounced in the intermediate gap zone i.e.at some distance from both disks. The

compaction in nano-particle profiles with strong suction may be attributable to the greater organization of the adsorption layer around the nanoparticle, which promotes the nano-lubricant molecules arrangement and this will inevitably contribute to enhanced lubricant film strength and load-carrying capacity.

5. CONCLUSIONS

A mathematical model has been presented for the laminar, squeezing hydrodynamics, heat and mass transfer in magnetic nanofluid bio-tribological film flow between two approaching disks, the upper descending and the lower stationary. Wall suction/injection i.e. mass flux characteristics at the lower disk have been incorporated. The nano-lubricant is composed of suspension of metal oxide nanoparticles with an electrically-conducting base fluid. The Buongiornio model has been employed to simulate nanoparticle Brownian motion and thermophoresis effects, for the case of dilute nanofluid lubricants. The non-dimensional momentum, heat and species (nano-particle) conservation equations are solved as an ordinary differential boundary value problem, subject to physically viable boundary conditions, using an efficient, stable B-spline collocation numerical method. The influence of squeeze number, Hartmann (magnetic body force) number, disk surface transpiration parameter, Brownian motion parameter and thermophoretic parameter are explored. Solutions are validated with the earlier homotopy method results of Hashmi *et al.* [25]. The present computations have shown:

(i)Increasing Hartmann number (magnetic field parameter) causes strong retardation in the radial flow with suction present at the lower disk, whereas with injection present (wall blowing at the lower disk), a weak acceleration in the radial flow is generated. Increasing Hartmann number also lowers nano-particle concentration, when suction is present at the lower disk, whereas it slightly enhances concentration of nano-particles for the case of wall injection at the lower disk.

(ii) Increasing Brownian motion parameter and also suction or injection at the lower disk serve to increase temperature in the nano-lubricant, although much greater magnitudes are achieved with injection. Nano-particle concentrations are also enhanced with greater Brownian motion parameter when wall injection is present, but reduced when wall suction is imposed at the lower disk.

(iii) Increasing thermophoresis parameter effectively enhances nano-particle concentrations near the lower disk when wall suction is present, whereas the reverse trend is observed when wall injection is present at the lower disk and the decrease is most pronounced near the upper disk. Temperature is also increased with greater thermophoretic effect, both when suction or injection are prescribed at the lower disk, although lower temperatures (enhanced cooling of the squeeze film) is achieved with suction.

(iv)With increasing squeeze film parameter, there is a substantial reduction in temperatures and increasing suction effect at the disk also results in lesser temperature magnitudes i.e. more effective cooling of the nano-lubricant squeeze film. A substantial decrease in nano-particle concentration is also accompanied with increasing squeeze film parameter with lower disk wall suction whereas with wall injection, the contrary trend is found and nano-particle concentration magnitudes are markedly enhanced.

The present simulations provide a first step towards more generalized squeeze film nano-bio-lubricant dynamics. Non-Newtonian effects have been neglected in the current model and these are currently being explored using couple stress, micropolar and also viscoelastic models, which may provide deeper insight into nano-lubricant rheology.

REFERENCES

[1] S.U.S. Choi, Enhancing thermal conductivity of fluids with nanoparticle, in: *D.A. Siginer, H.P. Wang (Eds.), Developments and Applications of Non-Newtonian Flows, Vol. FED 231, ASME, New York*, 1995, pp. 99–105.

[2]Y. Hwang, H.S. Park, J.K. Lee and W.H. Jung, Thermal conductivity and lubrication characteristics of nanofluids, *Current Applied Physics*, 6 (2006) e67–e71.

[3] B. Shen, Albert J. Shih and Simon C. Tung, Application of nanofluids in minimum quantity lubrication grinding, *Tribology Transactions*, 51 (2008) 730-737.

[4] S. Khandekar, M. Ravi Sankar, V. Agnihotri & J. Ramkumar, Nano-cutting fluid for enhancement of metal cutting performance, *Materials and Manufacturing Processes*, 27 (2012) 963-967.

[5] Cong Mao, Yong Huang, Xin Zhou, Hangyu Gan, Jian Zhang, Zhixiong Zhou, The tribological properties of nanofluid used in minimum quantity lubrication grinding, *The Int. J. Advanced Manufacturing Technology*, 71 (2014) 1221-1228.

[6] Alice Pendleton; Prasenjit Kar; Subrata Kundu; Sahar Houssamy; Hong Liang, effects of nanostructured additives on boundary lubrication for potential artificial joint applications, *ASME J. Tribol.,* 132 (2010) 031201-031201-5.

[7] Rashmi R. Sahoo, Sanjay K. BiswasR. R. Sahoo and S. K. Biswas, Deformation and friction of MoS2 particles in liquid suspensions used to lubricate sliding contact, *Thin Solid Films* 518, 5995 (2010).

[8] R. Nicoletti, The importance of the heat capacity of lubricants with nanoparticles in the static behavior of journal bearings, *ASME J. Tribol*., 136(2014) 044502-044502-5.

[9] Harta, I., Owens, K., De Jesús Santiago, S., Schall, D. et al., Tribological performance of ZnO-oil nanofluids at elevated temperatures, *SAE Int. J. Fuels Lubr.* 6 (2013) 126-131, 2013.

[10] D. T. Wasan and Alex D. Nikolov, Spreading of nanofluids on solids, *Nature* 423 (2003) 156-159.

[11] K.G. Binu, B.S. Shenoy, D.S. Rao, R. Pai, Static characteristics of a fluid film bearing with TiO2 based nanolubricant using the modified Krieger–Dougherty viscosity model and couple stress model, *Tribology International*, 75 (2014) 69-79.

[12] Z.Y. Xu, Y. Xu, K.H. Hu, Y.F. Xu, X.G. Hu, , Formation and tribological properties of hollow sphere-like nano-MoS_2 precipitated in TiO_2 particles, *Tribology International*, 81 (2015) 139–148.

[13] Aditya Kumar, Bharat Bhushan, Nanomechanical, nanotribological and macrotribological characterization of hard coatings and surface treatment of H-13 steel, *Tribology International*, 81 (2015) 149–158.

[14] F. Niyaghi, Karl R. Haapala, Stacey L. Harper and Michael C. Weismiller, Stability and biological responses of zinc oxide metalworking nanofluids using dynamic light scattering and zebrafish assays, *Tribology Transactions*, 57 (2014) 730-739.

[15] Hamed Ghaednia, Robert L. Jackson & Jeyhoon M. Khodadadi, Experimental analysis of stable CuO nanoparticle enhanced lubricants, *J. Experimental Nanoscience*, 10 (2015) 1-18.

[16] Yonghai Kang, Jun Yang, Licai Fu, Jiqiang Ma, Qinling B, Weimin Liu, Tribological behavior of $Fe_{70}Ni_{30}$ alloy with nanoscale twins under liquid paraffin lubrication, *Proc. IMechE-Part J: J. Engineering Tribology,* 227 (2013) 60-66.

[17] T. Hayat, M. Nawaz, A. A. Hendi and S. Asghar, MHD squeezing flow of a micropolar fluid between parallel disks, *ASME J. Fluids Eng*., 133 (2011) 111206.

[18] O. Anwar Bég, D. Tripathi, T. Sochi and PK Gupta, Adomian decomposition method (ADM) simulation of magneto-bio-tribological squeeze film with magnetic induction effects, *J. Mechanics Medicine Biology,* 15, 1550072.1-1550072.23 (2015).

[19] M Daliri, D Jalali-Vahid and H Rahnejat, Squeeze film lubrication of coupled stress electrically conducting inertial fluids in wide parallel rectangular conjunctions subjected to a magnetic field, *Proc. IMechE.-Part J: J. Engineering Tribology,* 228 (2014) 288-302.

[20] J. Zueco and O. Anwar Bég, Network numerical analysis of hydromagnetic squeeze film flow dynamics between two parallel rotating disks with induced magnetic field effects, *Tribology International*, 43, 532-543 (2010).

[21] T. Hayat, Arshia Yousaf, M. Mustafa and S. Obaidat, MHD squeezing flow of second-grade fluid between two parallel disks, *Int. J. Numerical Methods in Fluids*, 69 (2012) 399–410.

[22] O. Anwar Bég, R. Bhargava, S. Singh and H. Maregere, Element-Free Galerkin method (EFGM) computation of transient micropolar magnetic squeeze film flow, *Int. J. Applied Mathematics and Mechanics,* 16, 1-21 (2013).

[23] J. Wang, N. Feng, G. Meng and E. J. Hahn, Vibration control of rotor by squeeze film damper with magnetorheological fluid, *J. Intelligent Material Systems and Structures*, 17 (2006) 353-357.

[24] C Carmignani, P Forte and E Rustighi, Design of a novel magneto-rheological squeeze-film damper, *Smart Mater. Struct.*, 15 (2006) 164–170.

[25] M.M. Hashimi, T. Hayat and A. Alsaedi, On the analytic solutions for squeezing flow of nanofluid between parallel disks, *Nonlinear Analysis: Modelling and Control*, 17 (2012) 418-430.

[26] K.P. Gertzos, P.G. Nikolakopoulos and C.A. Ppadopoulos, CFD analysis of journal bearing hydrodynamic lubrication by Bingham lubricant, *Tribol. International*, 41 (2008) 1190-1204.

[27] O. Anwar Bég, T.A. Bég, Ferromagnetic "intelligent" dampers for infrastructural and medical systems, *Technical Report, FERRO-A-413/May, Gort Engovation, Bradford/Narvik/Stockholm, 115 pages, May* (2013).

[28] K. Zakaria, Sirwah MA, Fakharany M, Theoretical study of static and dynamic characteristics for eccentric cylinders lubricated with ferrofluid, *ASME J Tribol* 133 (2011) 021701.

[29] M.E. Davis, *Numerical methods and modeling for chemical engineers*. Courier Corporation (2013).

[30] W. Zhao, Ying Wang, Liping Wang, Mingwu Bai and Qunji Xue, Influence of heat treatment on the micro/nano-tribological properties of ultra-thin ionic liquid films on silicon, *Colloids and Surfaces A Physicochemical and Engineering Aspects* 361(1-3):118-125 (2010).

[31]S. Mivake, M. Wang, S. Ninomiya, Nanotribological properties of perfluoropolyether-coated magnetic disk evaluated by vertical and lateral vibration wear tests, *Surf. Coat. Technol*. 200 (2006) 6137–6154.

[32]W. Liu and Xiaobo Wang, Nanolubricants made of metals, pp. 175-201, In *Nanolubricants, Edited by Jean Michel Martin and Nobuo Ohmae*, John Wiley and Sons, UK (2008).

[33] D.P. Kulkarni, Das, D.K. and Chukwu, G.A. Temperature dependent rheological property of copper oxide nanoparticles suspension (nanofluid). *J. Nanosci. Nanotechnol.* 6, 1150–1154 (2006).

[34] Ghaednia, H., Jackson, R.L., and Khodadadi, J.M. Experimental analysis of stable cuo nanoparticle enhanced lubricants, *J. Experimental Nanoscience*, 8, 1-18 (2013)

[35] G. Vakili-Nezhaad and A. Dorany, Effect of single-walled carbon nanotube on the viscosity of lubricants, *Energy Procedia*, 14, 512–517 (2012).

[36] C. Hu, M. Bai, J. Lv, X. Li, Molecular dynamics simulation of mechanism of nanoparticle in improving load-carrying capacity of lubricant film, *Computational Materials Science,* 109, 97–103 (2015).